Endochondral bone in an Early Devonian 'placoderm' from Mongolia

Martin D. Brazeau[1,2]*, Sam Giles [2,3,4], Richard P. Dearden[1,5], Anna Jerve[1,6], Y.A. Ariunchimeg[7], E. Zorig[8], Robert Sansom[9], Thomas Guillerme[10], Marco Castiello[1]

[1] *Department of Life Sciences, Imperial College London, Silwood Park Campus, Buckhurst Rd, Ascot, SL5 7PY, UK;*

[2] *Department of Earth Sciences, Natural History Museum, Cromwell Road, London SW7 5BD, UK;*

[3] *School of Geography, Earth and Environmental Sciences, University of Birmingham, Birmingham, UK;*

[4] *Department of Earth Sciences, University of Oxford, South Parks Road, Oxford, OX1 3AN, UK;*

[5] *CR2P Centre de Recherche en Paléontologie – Paris, Muséum national d'Histoire naturelle, Sorbonne Universités, CNRS, CP 38, 57 Rue Cuvier, 75231, Paris, Cedex 05, France*

[6] *Department of Organismal Biology, Subdepartment of Evolution and Development, Uppsala University, Norbyvägen 18A, 752 36 Uppsala, Sweden;*

[7] *Natural History Museum, P.O. Box 46/52, Ulaanbaatar 1420, Mongolia*

[8] *Institute of Paleontology, Mongolian Academy of Science, P.O. Box 46/650, S. Danzan Street 3/1, Chingeltei District. Ulaanbaatar 15160, Mongolia;*

[9] *School of Earth and Environmental Sciences, University of Manchester, Manchester M13 9PT, UK;*

[10] *Department of Animal and Plant Sciences, The University of Sheffield, Sheffield S10 2TN, UK;*

* Author for correspondence.

Endochondral bone is the main internal skeletal tissue of nearly all osteichthyans—the group comprising more than 60,000 living species of bony fishes and tetrapods. Chondrichthyans (sharks and their kin) are the living sister group of osteichthyans and have cartilaginous endoskeletons, long considered the ancestral condition for all jawed vertebrates (gnathostomes). The absence of bone in modern jawless fishes and the absence of endochondral ossification in early fossil gnathostomes appears to lend support to this conclusion. Here we report the discovery of extensive endochondral bone in *Minjinia turgenensis*, a new genus and species of 'placoderm'-like fish from the Early Devonian (Pragian) of western Mongolia described using x-ray computed microtomography (XR-µCT). The fossil consists of a partial skull roof and braincase with anatomical details providing strong evidence of placement in the gnathostome stem group. However, its endochondral space is filled with an extensive network of fine trabeculae resembling the endochondral bone of osteichthyans. Phylogenetic analyses place this new taxon as a proximate sister group of the gnathostome crown. These results provide direct support for theories of generalised bone loss in chondrichthyans. Furthermore, they revive theories of a phylogenetically deeper origin of endochondral bone and its absence in chondrichthyans as a secondary condition.

The vertebrate skeleton comprises two main systems: the exoskeleton (external achondral dermal bones) and endoskeleton (internal chondral bones and cartilages, as well as some intramembranous bones)[1]. An ossified exoskeleton evolved at least 450 million years ago in jawless stem gnathostomes[2,3], but the endoskeleton in these taxa is not endochondrally ossified. Endochondral bone, in which the cartilaginous endoskeletal precursor is invaded by and eventually replaced by bone, is widely considered an osteichthyan apomorphy[3-7] and such a reliable identifying character gives the group its name. Extant chondrichthyans lack

53 dermal bone and possess a mainly cartilaginous endoskeleton enveloped by a structurally
54 diverse range of tessellate calcified cartilage[8]. Outgroups of the gnathostome crown also lack
55 endochondral ossification. Galeaspids surround their cartilaginous skeleton in globular
56 calcified cartilage{NianZhong:2005tj}, while osteostracan and 'placoderm' endoskeletons
57 were sheathed in perichondral bone[3]. Consequently, the last common ancestor of jawed
58 vertebrates was long thought to have been perichondrally ossified, but lacking endochondral
59 ossification[3].
60 In this paper, we describe a new genus and species of 'placoderm' from the Early
61 Devonian of western Mongolia. Although Mongolia is known for some of the geologically
62 oldest putative gnathostome fossils (isolated chondrichthyan-like scales [9-12]), it remains a
63 poorly sampled region of the world with respect to early vertebrates. 'Placoderms' were until
64 now known from only a single fragmentary occurrence[13] in the early Middle Devonian
65 (Eifelian). Our new data highlight the importance of Mongolia as a key region for studies of
66 early gnathostome evolution. We describe a braincase and partial skull roof representing the
67 first substantial body fossil of an early gnathostome from Mongolia and displaying an
68 unexpected occurrence of endochondral bone analysed using XR-µCT. We conducted
69 phylogenetic analyses to reconstruct the evolutionary relationships of this new taxon. To
70 explore the evolutionary history of endochondral bone in light of this new discovery, we used
71 parsimony and maximum likelihood ancestral states reconstruction. Finally, we discuss these
72 results in the context of earlier statements about endochondral bone in non-osteichthyans,
73 new developments in understanding the complexity and diversity of chondrichthyan
74 endoskeletal tissues, and current uncertainties about early gnathostome phylogenetic
75 relationships.
76
77 **Systematic palaeontology**

Gnathostomata Gegenbaur, 1874[14]

Minjinia turgenensis gen. et sp. nov.

Etymology. Generic name honours the memory of Chuluun Minjin for his extensive contributions to the Palaeozoic stratigraphy of Mongolia, his enthusiastic support of this work, and introducing us to the Yamaat River locality. Specific name recognises the provenance of the fossil from the Turgen region, Uvs aimag of western Mongolia.

Holotype. Institute of Paleontology, Mongolian Academy of Sciences MPC-FH100/9.1, a partial braincase and skull roof.

Type locality. Turgen Strictly Protected Area, Uvs province, western Mongolia; near the top of the stratigraphic sequence that occurs between the Tsagaan-Salaat and Yamaat Rivers.

Formation and age. Upper part of Tsagaansalaat Formation, Pragian (Early Devonian) [15,16].

Diagnosis. 'Placoderm'-grade stem gnathostome with endochondral bone, deep epaxial muscle cavities flanking a slender occipital ridge, and the following possible autapomorphies: dermal bones covered in sparsely placed tubercles, penultimate spino-occipital nerve canal substantially larger in diameter than others.

Description

MPC-FH100/9.1 consists of a partial braincase and skull roof (Fig. 1). The skull roof is ornamented with sparsely distributed finely ridged tubercles resembling those of the Siberian 'placoderm' *Dolganosteus*[17]; the tubercles become more broadly separated towards the

103 midline of the skull. They are distinct from those of *Dolganosteus* in that towards the midline
104 of the skull roof, the tubercles are larger and more pointed. The specimen shows signs of
105 extensive post-mortem transport, with angles of the braincase worn off and much of the skull
106 roof and some of the braincase preserved as a mould. Individual skull roof ossifications
107 cannot be identified, although this may be due to the dominantly mouldic preservation. There
108 appears to have been a prominent nuchal plate eminence comparable to certain
109 acanthothoracids such as *Romundina*[18] and *Arabosteus*[19].
110
111 **Endoskeletal tissue.** The braincase of MPC-FH100/9.1 is well ossified, comprising an
112 external bony sheath filled with an extensive matrix of spongy tissue (Fig. 2a-b; Extended
113 Data Fig. 1; Supplementary Video 1). The trabecles forming this tissue are irregular and
114 branching, less than 1 mm thick and often curved, and resemble most closely the
115 endochondral tissue of osteichthyans (Fig. 2c-d; Supplementary Video 2). As such, we
116 interpret this as endochondral bone. Notably, this is found in all preserved regions of the
117 braincase, in contrast to the isolated trabeculae previously identified as endochondral bone in
118 *Boreaspis*[20] and *Bothriolepis*[21]. The margins of the braincase, the endocranial walls, and the
119 boundaries of nerve and blood canals, are formed from a thicker tissue which we interpret as
120 perichondral bone. This suggests that the endoskeleton of *Minjinia* comprises osteichthyan-
121 like endochondral bone, with an ossified perichondrium. To address the possible alternative
122 explanation that it is an aberrant instance of calcified cartilage, we compared the structure of
123 this tissue with rarely-preserved mineralized cartilage in the stem chondrichthyan
124 *Diplacanthus crassismus* (National Museums of Scotland specimen NMS 1891.92.334; Fig.
125 2e-f) observed using synchrotron tomography. The cancellae within the endochondral tissue
126 of *Minjinia* are irregular, with a diameter of approximately 1-2 mm. This tissue is distinctly

127 unlike the calcified cartilage of *Diplacanthus* in appearance, which consists of a densely
128 packed matrix of irregularly stacked chondrons between 20-60 μm in diameter.
129
130 **Neurocranium.** The braincase is preserved from the level of the right posterior orbital wall
131 to the posterior end of the occipital ridge. Occipital glenoid condyles are not preserved, but
132 much of the rest of the broad, flat parachordal region is present, separated by a midline
133 groove that accommodated a relatively narrow notochordal tunnel. An asymmetric transverse
134 fissure spans the basicranial surface at about mid-length of the preserved portion. It appears
135 to demarcate the anterior margin of the parachordal plates and may correspond to the ventral
136 cranial fissure of crown-group gnathostomes. However, unlike in crown gnathostomes, it is
137 traversed by a substantial anterior extension of the cranial notochord. The courses of the
138 lateral dorsal aortae are marked by a pair of sulci on the lateral margins of the parachordal
139 plates, though only a short part of the canal is preserved on the right side of the specimen. A
140 narrow, shallow sulcus for the efferent hyoid artery is present on the preserved right side of
141 the specimen, immediately behind the level of the orbit (Fig. 1a).
142 The lateral surface of the braincase is preserved on the right side as a mouldic
143 impression in the matrix (Fig. 1). A sharply demarcated hyoid fossa is present on the lateral
144 wall of the otic region (Fig. 1). Posterior to this, a stout but pronounced vagal process with a
145 pair of rounded eminences likely corresponds to the branchial arch articulations. There is no
146 evidence for a pair of anterior and posterior divisions to the vagal process, which are
147 typically seen in other 'placoderms'. A well-developed 'placoderm'-like craniospinal
148 process is absent; its homologous position is instead covered in perichondral bone and
149 marked by a low ridge (Fig. 1).
150 In posterior view, a tall, narrow median occipital ridge is evident and resembles the
151 morphology of *Romundina*[22] and *Arabosteus*[19]. Similar to these taxa, the median otic ridge is

152 flanked by two large occipital fossae for the epaxial musculature. The notochordal tunnel is
153 approximately the same size as or smaller than the foramen magnum, as in 'placoderms' and
154 in contrast with crown-group gnathostomes. A metotic fissure is absent.
155
156 **Endocast.** A partial cranial endocast is preserved, consisting of the hindbrain cavity, partial
157 midbrain cavity, labyrinth cavities, and posteromedial corner of the orbital region. The two
158 primary trunk canals of the trigeminal nerve ($N.V_1$ and $N.V_{2,3}$) are preserved (Fig. 3). The
159 acoustic (N.VIII) and facial nerve (N.VII) canals share a common trunk canal behind the
160 trigeminal nerves, as in many other 'placoderms' [22-25]. The facial nerve canal branches into
161 palatal and hyomandibular branches between the saccular chamber and rear orbit wall (Fig. 3;
162 Extended Data Fig. 2), indicating this division was internal (deep) to the otic process. The
163 supraophthalmic branch opens into the rear wall of the orbit and part of its supraorbital
164 course is preserved (Fig. 3; Extended Data Fig. 2). A slender branch extends below the
165 labyrinth and divides into palatine and hyomandibular branches (Fig 3; Extended Data Fig.
166 2). As in other 'placoderm'-grade taxa, the vagus nerve (N. X) trunk canal is very large in
167 diameter and exits from immediately behind the labyrinth cavity (Fig. 3). The spino-occipital
168 region resembles other 'placoderms' in being extended. At least four spino-occipital nerve
169 canals are present in a linear series, and the penultimate canal is largest in diameter (Fig. 3).
170 Intercalating these is a network of occipital artery canals branching from the dorsal aortae.
171 The skeletal labyrinth is not complete on either side of the specimen, but can mostly
172 be reconstructed according to the assumption of bilateral symmetry. The most significant
173 feature is that the labyrinth and endolymphatic cavity are joined to the main endocavity
174 chamber (Fig. 3). This is a striking contrast to other 'placoderms' and closely resembles
175 crown-group gnathostomes[26]. The endolymphatic canals are elongate and tubular, extending
176 posterolaterally to reach the skull roof, though external openings cannot be clearly identified.

177 The anterior semi-circular canal follows the saccular cavity closely as in petalichthyids[27](Fig.
178 3). However, the horizontal and posterior canals appear to extend well away from the
179 saccular chamber (Fig. 3). The dorsal junctions of the anterior and posterior canals are joined
180 in a crus commune, as in *Romundina*[22] and *Jagorina*[23]. A sinus superior is absent.
181
182 **Phylogenetic analyses**
183 We conducted phylogenetic analyses under four different protocols: equal weights
184 parsimony, implied weights parsimony, an unpartitioned Bayesian analysis, and a Bayesian
185 analysis with characters partitioned by fit determined under implied weights parsimony[28] (see
186 Extended Data Figs. 3-6). All phylogenetic analyses consistently place *Minjinia* as a stem-
187 group gnathostome, proximate to the gnathostome crown (Fig. 4, Extended Data Figs 3, 4).
188 *Minjinia* is recovered in a position crownward of arthrodires but outside of a grade consisting
189 of *Entelognathus*, *Ramirosuarezia*, and *Janusiscus*. Under implied weights parsimony, these
190 three taxa move onto the osteichthyan stem and *Minjinia* is placed as the immediate sister
191 taxon of the gnathostome crown. Under parsimony, the crownward position of *Minjinia* is
192 unambiguously supported by the skeletal labyrinth and endolymphatic duct being confluent
193 with the main cranial cavity[26] (Supplementary Information). In common with arthrodires and
194 the gnathostome crown[29], *Minjinia* possesses a division of the facial nerve(Fig. 3; Extended
195 Data Fig. 2) deep to the transverse otic process. However, *Minjinia* is excluded from the
196 gnathostome crown group due to the absences of a metotic fissure and a posterior dorsal
197 fontanelle, and presence of broad, flat parachordal plates expanded behind the saccular cavity
198 (Fig. 3, Supplementary Information).
199 We undertook ancestral states reconstructions to assess the evolutionary history of
200 endochondral bone (Fig. 4; Extended Data Figs. 5 & 6; Supplementary Information).
201 Interestingly, parsimony analysis fails to recover secondary homology of this trait between

202 *Minjinia* and osteichthyans. The crownward placement of *Minjinia* is, in fact, based on
203 independent evidence relating to anatomical features of the braincase and endocast. However,
204 the resolution becomes ambiguous if missing data in either *Entelognathus* or *Ramirosuarezia*
205 are resolved as having endochondral bone. The reconstruction becomes similarly ambiguous
206 if *Janusiscus* is moved a single branch (requiring only two additional steps) onto the
207 chondrichthyan stem. The strict precision of parsimony reconstructions makes it insensitive
208 to this underlying uncertainty. To explore this, we used likelihood reconstructions and
209 compared the ancestral state reconstructions under equal rates (ER) and all rates different
210 (ARD) variants of the Mkv model on branch-length-rescaled parsimony trees and Bayesian
211 trees. Both models show substantial non-zero marginal likelihoods if endochondral bone is
212 assumed present in the common node of *Minjinia* and Osteichthyes, with ARD strongly
213 favouring its presence (0.33 for ER; 0.81 for ARD; Fig. 3, Table 1, Extended Data Figs. 5, 6,
214 Supplementary Table 1). Under the ARD model, there is nearly equivocal support for
215 presence or absence of endochondral bone at the gnathostome crown node (Table 1). The
216 ARD model shows the best fit for endochondral bone (likelihood ratios 4.75 for parsimony [p
217 = 0.029] and 5.26 for Bayesian, [p = 0.022]) (Table 1, Supplementary Table 1), favouring
218 repeated losses of this tissue over multiple gains (see Discussion).
219
220 **Discussion**
221 *Minjinia turgenensis* presents an unexpected discovery of extensive endochondral bone in a
222 'placoderm'-grade fish, with repercussions for the phylogenetic origin of this tissue and the
223 problem of early gnathostome relationships more generally. The prevailing hypothesis has
224 been that endochondral bone is an osteichthyan apomorphy[3,7,29]. However, recent discoveries
225 have cast doubt on this assertion. The recognition that dermal bone is secondarily lost in
226 chondrichthyans[30,31] (Fig. 4) is consonant with prior knowledge of the loss of perichondral

227 bone in this same lineage[32]. Taken together, this has revived uncertainty about the true
228 phylogenetic timing of the origin of endochondral ossification[33]. *Minjinia* provides direct
229 corroboration for a more ancient origin.

230 *Minjinia* does not represent the first report of endochondral bone outside of
231 Osteichthyes. However, it is by far the most extensive and unequivocal example and raises
232 explicit questions in light of the proximity of *Minjinia* to the gnathostome crown (Fig. 4;
233 Extended Data Figs. 3, 4). Isolated examples of trabecular endoskeletal bone have historically
234 been reported in boreaspid osteostracans[20,34], a rhenanid[35], arthrodires[36], a ptyctodont[37], and a
235 petalichthyid[38,39]. However, these reports are nearly all unillustrated statements; they have all
236 been considered tenuous[3] or dismissed as misidentifications[5]. In line with these assessments,
237 we found no evidence of endochondral bone in material of *Buchanosteus* held in the Natural
238 History Museum, London, or indeed in any other 'placoderms' we have examined. The
239 *Epipetalichthys* holotype (Museum für Naturkunde, Berlin specimen MB.f.132.1-3) shows an
240 apparently spongiose infilling in the anterior region of the braincase, but the identity of this
241 structure, or even whether it is biological, cannot be determined. The *Epipetalichthys* tissue
242 figured by Stensiö[38] was very superficial, and possibly represents the retreat of perichondral
243 bone deposited during cartilage growth[39]. Most recently, trabeculae in supposed endoskeletal
244 pelvic bones of *Bothriolepis* have been termed endochondral bone[21], although the small scale
245 of these is in line with 'superficial' perichondral trabeculae seen elsewhere[38]. The reported
246 examples in boreaspid osteostracans have also been dismissed by later authors[3,5]. Although
247 they warrant further study, their tissue structures are unlikely to be homologous to
248 osteichthyans owing to their phylogenetic remoteness and nested position in the
249 Osteostraci[40].

250 Among chondrichthyans, endochondral bone has been mentioned in 'acanthodians'[3,41]
251 and superficial bone-like tissues have been reported in the skeletons of extant

chondrichthyans. We are unable to substantiate statements about acanthodians: no authors have cited primary sources or specimens. One possible source is Watson's[42] description of "massive ossification" of the endoskeleton of *Diplacanthus*. However, our synchrotron data of this same specimen (Fig. 2) shows that this tissue is undoubtably calcified cartilage. Some authors have speculated that the superficial mineralised tissue in the jaws of acanthodians or chondrichthyans may have developed in an endochondral position[39]. Histological studies show that endoskeletal mineralization in the jaws of acanthodians is globular calcification and occasionally 'sub-tessellate'[8,43]. Recent comparative histology and development in extant chondrichthyans has shown the presence of an extensive canalicular network in the tesserae[44] and a trabecular tesseral network in some vertebral elements[45], both resembling bone. Whether these represent homologues of osteichthyan examples remains open to debate; future works could employ synchrotron microtomography of stem-chondrichthyan cartilages to address these questions.

Does endochondral bone have a deep origin within the gnathostome stem group? This would imply repeated losses of this tissue. We do find statistical support for this hypothesis (Fig. 4, Table 1, Extended Data Figs. 5, 6, Supplementary Table 1), and the model is well justified on prior phylogenetic and biological grounds. Endochondral bone has long been known to be inconsistently developed across 'primitive' bony fishes: incomplete, polymorphic, or entirely absent ossification of the endoskeleton is known in both Palaeozoic actinopterygians[41,46,47] and sarcopterygians{Cloutier:wm}, as well as more recent taxa[48]. The frequent absence of endochondral bone in osteichthyans is considered secondary, and other controlling factors such as body size, maturity, mechanical stress, and buoyancy can determine its degree of development[1]. Our findings are also in agreement with studies establishing a genetic basis for secondary loss of all bone types within chondrichthyans[49-51],

with the failure to produce endochondral bone likely representing arrested development of chondrocytes as opposed to a primary lack of ability[52].

Another confounding factor in this question is the problem of 'placoderm' relationships. Although currently resolved in most analyses as a deeply pectinate grade along the gnathostome stem (Fig. 4), the backbone of this arrangement has poor statistical support, even in the present analysis (Extended Data Figs. 3). There is a lack of consistency in the arrangement of plesia and Bayesian tip-dating methods have even recovered a monophyletic Placodermi[53]. *Minjinia* itself highlights this uncertainty, given its highly unexpected character combinations. Notwithstanding its endochondral bone and crown-gnathostome-like inner ear structure, it resembles 'acanthothoracids'—the 'placoderms' widely considered among the most removed from the gnathostome crown (i.e. most 'primitive'): it possesses deep epaxial fossae either side of a prominent occipital ridge and a nuchal eminence otherwise seen only in acanthothoracids such as *Romundina*[18] and *Arabosteus*[19]. This apparent character conflict could perhaps be more easily reconciled with a more coherent (though not necessarily monophyletic) 'placoderm' assemblage. Indeed, the highly pectinate structure of the 'placoderm' grade seems symptomatic of an overemphasis on characters and taxa resembling the crown group, thereby undersampling characters that could stabilise a clear picture of 'placoderm' interrelationships.

Minjinia turgenensis reveals new data on 'placoderm' endoskeleton and tissue diversity recorded from Mongolia—an otherwise extremely poorly known biogeographic realm for early gnathostomes. The phylogenetic placement of this 'acanthothoracid'-like taxon crownward of all non-maxillate 'placoderms', in conjunction with possession of extensive endochondral bone, highlights the importance of material from traditionally undersampled geographic areas. The presence of endochondral bone renews the hypothesis that this tissue is evolutionarily ancient and was lost secondarily in chondrichthyans[6,33]. This

301 view is overall consistent with evidence of generalised bone loss in chondrichthyans,
302 potentially as a result of the suppression of bone-generating molecular genetic pathways[51,52].
303 Continued work in Mongolia and re-evaluation of phylogenetic datasets will be necessary to
304 address this, with the results likely to lead to substantial re-evaluation of gnathostome
305 phylogeny.
306
307
308 **Methods**
309
310 **X-ray computed microtomography.** We scanned MPC-FH100/9.1 using the Nikon XT
311 225s at the Museum of Paleontology, University of Michigan with the following parameters:
312 200kV, 140μA, over 3123 projections and a voxel size of 32.92μm. We conducted
313 segmentation using Mimics 19.0 (http://biomedical.materialise.com/mimics; Materialise,
314 Leuven, Belgium) and we imaged models for publication using Blender
315 (https://www.blender.org).
316 **Synchrotron light propagation phase contrast tomography.** We imaged *Diplacanthus*
317 *crassismus* specimen NMS 1891.92.334 on Beamline 19 of the European Synchrotron
318 Radiation Facility, using propagation phase-contrast synchrotron microtomography. We
319 performed a spot scan with an energy of 116keV, achieving a voxel size of 0.55 μm. We
320 processed the resulting tomograms using VG StudioMax 2.2 (Volume Graphics, Germany),
321 and prepared images in Blender.
322 **Phylogenetic analysis.** We conducted a parsimony analysis using TNT 1.5[54] and Bayesian
323 analysis using MrBayes v 3.2.7[55]. The dataset consisted of 95 taxa and 284 discrete
324 characters based on a pre-existing dataset[56]. We employed Osteostraci and Galeaspida as
325 composite outgroups. We conducted parsimony analysis using both equal weights and

326 implied weights methods. Global settings were 1000 search replicates and a hold of up to 1
327 million trees. Equal weights parsimony analyses were conducted using the ratchet with
328 default settings. Implied weights parsimony used a concavity parameter of 3 and the search
329 was without the ratchet. Command lists are included in Supplementary Information. We
330 conducted Bayesian analysis using both a partitioned and unpartitioned dataset. We used the
331 Mkv model[57] and gamma rate distribution. We ran the analyses for 5 million generations with
332 a relative burn-in fraction of 0.25. Runs were checked for convergence using Tracer[58]. We
333 partitioned the dataset using a newly proposed method[28] that partitions the data according to
334 homoplasy levels. Using the results of implied weights parsimony conducted in TNT, we
335 created a text table of character fit values. We wrote an R[59] script to generate a list of
336 partition commands for MrBayes.

337 We assessed parsimony ancestral states visually using Mesquite[60]. Likelihood and
338 Bayesian ancestral states were estimated in R using the castor package[61] version 1.5.7. Prior
339 to calculating likelihood ancestral states on parsimony trees, we scaled branch lengths using
340 PAUP*[62] and calculated the likelihood scores for all of the trees under the Mkv model with
341 gamma rate parameter. The trees were then exported with branch lengths. To account for
342 overall uncertainty in tree estimates, we estimated ancestral states on 100 trees randomly
343 selected from the fundamental set of most parsimonious trees and two times 50 trees selected
344 from the 75% last trees of each posterior tree distribution from the Bayesian analysis. We
345 then run an ancestral states estimation Mk model (using the castor R package) using both the
346 Equal Rates (ER) and All Rates Different (ARD) models. This resulted in 400 ancestral states
347 estimations. For each estimation we extracted the overlap log likelihood, the AIC (counting
348 one parameter for the ER model and two for the ARD model) and the scaled log likelihood
349 (probability) for the presence and absence of the endochondral bone character (character 4)
350 for the last common node of *Minjinia* and crown-group gnathostomes. We present the median

value of these distributions of the estimations overall log likelihoods, AICs and presence or absence of endochondral bone in Table 1.

Data availability

The holotype specimen of *Minjinia turgenensis* will be permanently deposited in the collections of the Institute of Paleontology, Mongolian Academy of Sciences. Original tomograms are available at (doi:10.6084/m9.figshare.12301229) and rendered models are available at (doi:10.6084/m9.figshare.12301223). The phylogenetic character list and dataset are available as Supplementary Information S1 and S2. The LifeScience Identifier for *Minjinia turgenensis* is urn:lsid:zoobank.org:act:82A1CEEC-B990-47FF-927A-D2F0B59AEA87

Code availability

R code for generating partitions based on character fits and code for likelihood ancestral states reconstructions and plots are available in the Supplementary Information.

References

1. Hall, B. K. *Bones and Cartilage*. (Academic Press, 2005).
2. Janvier, P. *Early Vertebrates*. (Oxford University Press, 1996).
3. Donoghue, P. C. J., Sansom, I. & Downs, J. P. Early evolution of vertebrate skeletal tissues and cellular interactions, and the canalization of skeletal development. *Journal of Experimental Zoology* **306B,** 278–294 (2006).
4. Rosen, D. E., Forey, P. L., Gardiner, B. G. & Patterson, C. Lungfishes, tetrapods, paleontology, and plesiomorphy. *Bull Am Mus Nat Hist* **167,** 159–276 (1981).

5. Gardiner, B. G. The relationships of the palaeoniscid fishes, a review based on new specimens of *Mimia* and *Moythomasia* from Upper Devonian of Western Australia. *Bull Br Mus nat Hist (Geol)* **37,** 173–428 (1984).

6. Maisey, J. G. Heads and tails: a chordate phylogeny. *Cladistics* **2,** 201–256 (1986).

7. Friedman, M. & Brazeau, M. A Reappraisal of the origin and basal radiation of the Osteichthyes. *J Vertebr Paleontol* **30,** 36–56 (2010).

8. Maisey, J. G., Denton, J. S. S., Burrow, C. & Pradel, A. Architectural and ultrastructural features of tessellated calcified cartilage in modern and extinct chondrichthyan fishes. *Journal of Fish Biology* **15,** 37–23 (2020).

9. Karatajūtė-Talimaa, V. & Novitskaya, L. *Sodolepis*—a new representative of Mongolepidida (Chondrichthyes?) from the lower Silurian of Mongolia. *Paleontologicheskii Zhurnal* **5,** 96–103 (1997).

10. Karatajūtė-Talimaa, V. & Novitskaya, L. *Teslepis*—a new representative of mongolepid elasmobranchs from the Lower Silurian of Mongolia. *Paleontologicheskii Zhurnal* **4,** 36–43 (1992).

11. Karatajūtė-Talimaa, V., Novitskaya, L. & Rozman, K. S. *Mongolepis*—a new lower Silurian genus of elasmobranchs from Mongolia. *Paleontologicheskii Zhurnal* **1,** 76–86 (1990).

12. Andreev, P. *et al.* The systematics of the Mongolepidida (Chondrichthyes) and the Ordovician origins of the clade. *PeerJ* **4,** e1850–e1850 (2016).

13. Vorobjeva, E. I. & Janvier, P. Observations to the note by E Vorobjeva: 'First discovery of Palaeozoic fishes on the territory of the Mongolian Republic'. *Palaeontology and Biostratigraphy of Mongolia*, Moscow, 3, 134-136 (in Russian). *Geobios* **17,** 379–380 (1984).

14. Gegenbaur, C. *Grundriss der vergleichenden Anatomie*. 1–680 (Wilhelm Engelmann, 1874).

15. Alekseeva, R. E., Mendbayar, B. & Erlanger, O. A. *Brachiopods and Biostratigraphy of the Lower Devonian of Mongolia*. **16,** (Nauka, 1981).

16. Alekseeva, R. E. *Devonian Biostratigraphy of Mongolia*. (Nauka, 1993).

17. Mark-Kurik, E. in *Morphology, Phylogeny and Paleobiogeography of Fossil Fishes* (eds. Elliott, D. K., Maisey, J., Yu, X. & Miao, D.) 101–106 (2010).

18. Ørvig, T. Description, with special reference to the dermal skeleton, of a new radotinid arthrodire from the Gedinnian of Arctic Canada. *Colloque international C.N.R.S. no. 218* 43–71 (1975).

19. Olive, S., Goujet, D., Lelièvre, H. & Janjou, D. A new Placoderm fish (Acanthothoraci) from the Early Devonian Jauf Formation (Saudi Arabia). *Geodiversitas* **33,** 393–409 (2011).

20. Wängsjö, G. The Downtonian and Devonian vertebrates of Spitsbergen. IX. *Norsk Polarinstitutt Skrifter* **97,** 1–611 (1952).

21. Charest, F., Johanson, Z. & Cloutier, R. Loss in the making: absence of pelvic fins and presence of paedomorphic pelvic girdles in a Late Devonian antiarch placoderm (jawed stem-gnathostome). *Biology Letters* **14,** 20180199 (2018).

22. Dupret, V., Sanchez, S., Goujet, D. & Ahlberg, P. E. The internal cranial anatomy of *Romundina stellina* Ørvig, 1975 (Vertebrata, Placodermi, Acanthothoraci) and the origin of jawed vertebrates—Anatomical atlas of a primitive gnathostome. *PLoS ONE* **12,** e0171241 (2017).

23. Stensiö, E. A. La cavité labyrinthique, l'ossification sclérotique et l'orbite de *Jagorina*. *Colloques internationaux du Centre national de la Recherche scientifique* **21,** 9–43 (1950).

24. Stensiö, E. A. Anatomical studies on the arthrodiran head. *K Sven Vetenskapsakad Handl* **9,** 1–419 (1963).

25. Goujet, D. *Les poissons placodermes du Spitsberg*. (Cahiers de Paléontologie, Editions du CNRS, 1984).

26. Davis, S. P., Finarelli, J. A. & Coates, M. I. *Acanthodes* and shark-like conditions in the last common ancestor of modern gnathostomes. *Nature* **486,** 247–250 (2012).

27. Castiello, M. & Brazeau, M. D. Neurocranial anatomy of the petalichthyid placoderm *Shearsbyaspis oepiki* Young revealed by X□ray computed microtomography. *Palaeontology* **61,** 369–389 (2018).

28. Rosa, B. B., Melo, G. A. R. & Barbeitos, M. S. Homoplasy-based partitioning outperforms alternatives in Bayesian analysis of discrete morphological data. *Systematic Biology* **54,** 373 (2019).

29. Brazeau, M. D. & Friedman, M. The characters of Palaeozoic jawed vertebrates. *Zool J Linn Soc* **170,** 779–821 (2014).

30. Zhu, M. *et al.* A Silurian placoderm with osteichthyan-like marginal jaw bones. *Nature* **502,** 188–193 (2013).

31. Giles, S., Friedman, M. & Brazeau, M. D. Osteichthyan-like cranial conditions in an Early Devonian stem gnathostome. *Nature* **520,** 82–85 (2015).

32. Miles, R. S. in *Interrelationships of Fishes* (eds. Greenwood, P. H., Miles, R. S. & Patterson, C.) 63–103 (Academic Press London, 1973).

33. Zhu, M. Bone gain and loss: insights from genomes and fossils. *Natl Sci Rev* **1,** 490–492 (2014).

34. Janvier, P. *Les céphalaspides du Spitsberg*. (Éditions du Centre National de la Recherche Scientifique, 1985).

35. Ørvig, T. Histologic studies of placoderms and fossil elasmobranchs. *Arkiv för Zoologi* **2,** 321–454 (1951).

36. Young, G. C. New information on the structure and relationships of *Buchanosteus* (Placodermi: Euarthrodira) from the Early Devonian of New South Wales. *Zool J Linn Soc* **66,** 309–352 (1979).

37. Miles, R. S. & Young, G. C. in *Problems in Vertebrate Evolution* (eds. Andrews, S. M., Miles, R. S. & Walker, A. D.) 123–198 (Academic Press, 1977).

38. Stensiö, E. A. On the head of the macropetalichthyids. *Field Museum of Natural History Publication Geological Series* **4,** 87–197 (1925).

39. Ørvig, T. Notes on some Paleozoic lower vertebrates from Spitsbergen and North America. *Norsk Geologisk Tidsskrift* **37,** 285–353 (1957).

40. Sansom, R. Phylogeny, classification and character polarity of the Osteostraci (Vertebrata). *Journal of Systematic Palaeontology* **7,** 95–115 (2009).

41. Schaeffer, B. The braincase of the holostean fish *Macrepistius*, with comments on neurocranial ossification in the Actinopterygii. *American Museum Novitates* **2459,** 1–34 (1971).

42. Watson, D. M. S. The acanthodian fishes. *Philosophical Transactions of the Royal Society of London. Series B, Biological Sciences* **228,** 49–146 (1937).

43. Burrow, C. J., Davidson, R. G., Blaauwen, den, J. L. & Newman, M. J. Revision of *Climatius reticulatus* Agassiz, 1844 (Acanthodii, Climatiidae), from the Lower Devonian of Scotland, based on new histological and morphological data. *J Vertebr Paleontol* **35,** e913421 (2015).

44. Dean, M. N., Socha, J. J., Hall, B. K. & Summers, A. P. Canaliculi in the tessellated skeleton of cartilaginous fishes. *Journal of Applied Ichthyology* **26,** 263–267 (2010).

45. Atake, O. J., Cooper, D. M. L. & Eames, B. F. Bone-like features in skate suggest a novel elasmobranch synapomorphy and deep homology of trabecular mineralization patterns. *Acta Biomaterialia* **84,** 424–436 (2019).

46. Pearson, D. M. & Westoll, T. S. The Devonian actinopterygian *Cheirolepis* Agassiz. *Transactions of the Royal Society of Edinburgh: Earth Sciences* **70,** 337–399 (1979).

47. Giles, S. *et al.* Endoskeletal structure in *Cheirolepis* (Osteichthyes, Actinopterygii), An early ray□finned fish. *Palaeontology* **58,** 849–870 (2015).

48. Grande, L. & Bemis, W. E. Osteology and Phylogenetic Relationships of Fossil and Recent Paddlefishes (Polyodontidae) with Comments on the Interrelationships of Acipenseriformes. *Memoir (Society of Vertebrate Paleontology)* **11 (Supplement to Number 1),** 1–121 (1991).

49. Eames, B. F. *et al.* Skeletogenesis in the swell shark *Cephaloscyllium ventriosum*. *Journal of Anatomy* **210,** 542–554 (2007).

50. Venkatesh, B. *et al.* Elephant shark genome provides unique insights into gnathostome evolution. *Nature* **505,** 174–179 (2014).

51. Ryll, B., Sanchez, S., Haitina, T., Tafforeau, P. & Ahlberg, P. E. The genome of *Callorhinchus* and the fossil record: a new perspective on SCPP gene evolution in gnathostomes. *Evolution & Development* **16,** 123–124 (2014).

52. Marconi, A., Hancock-Ronemus, A. & Gillis, J. A. Adult chondrogenesis and spontaneous cartilage repair in the skate, *Leucoraja erinacea*. *eLife Sciences* **9,** 2813 (2020).

53. King, B., Qiao, T., Lee, M. S. Y., Zhu, M. & Long, J. A. Bayesian morphological clock methods resurrect placoderm monophyly and reveal rapid early evolution in jawed vertebrates. *Systematic Biology* **66,** 499–516 (2016).

496 54. Goloboff, P. A. & Catalano, S. A. TNT version 1.5, including a full implementation of
497 phylogenetic morphometrics. *Cladistics* **32,** 221–238 (2016).
498 55. Ronquist, F. & Huelsenbeck, J. P. MrBayes 3: Bayesian phylogenetic inference under
499 mixed models. *Bioinformatics* **19,** 1572–1574 (2003).
500 56. Clement, A. M. *et al.* Neurocranial anatomy of an enigmatic Early Devonian fish sheds
501 light on early osteichthyan evolution. *eLife Sciences* **7,** e34349 (2018).
502 57. Lewis, P. O. A likelihood approach to estimating phylogeny from discrete
503 morphological character data. *Systematic Biology* **50,** 913 (2001).
504 58. Rambaut, A., Drummond, A. J., Xie, D., Baele, G. & Suchard, M. A. Posterior
505 summarization in Bayesian phylogenetics using Tracer 1.7. *Systematic Biology* **67,**
506 901–904 (2018).
507 59. R Core Team. *R: A language and environment for statistical computing.* (R
508 Foundation for Statistical Computing, 2019).
509 60. Maddison, D. R. & Maddison, W. P. *Mesquite*. (2019).
510 61. Louca, S. & Doebeli, M. Efficient comparative phylogenetics on large trees.
511 *Bioinformatics* **34,** 1053–1055 (2017).
512 62. Swofford, D. L. *PAUP**. 4.0a166, (2019).
513

514 **Acknowledgements.** M. Bolortsetseg generously assisted MDB with contacts and field
515 experience in Mongolia. Fieldwork was supported by National Geographic Society grants
516 CRE 8769-10 and GEFNE35-12 to MDB. AJ's field contributions were supported by funds
517 from the Anna Maria Lundin's stipend from Smålands Nation, Uppsala University. RS's field
518 contributions were supported by a Royal Society Research Grant and the University of
519 Manchester. The majority of this work was supported by the European Research Council
520 (ERC) under the European Union's Seventh Framework Programme (FP/2007-2013)/ERC

Grant Agreement number 311092 to MDB. RPD was also supported by the Île-de-France DIM (domaine d'intérêt majeur) matériaux anciens et patrimoniaux grant PHARE. Stig Walsh is thanked for access and loan of specimen at the National Museums of Scotland. Synchrotron tomography was performed at the ESRF (application LS 2451) with the assistance of Paul Tafforeau. SG was supported by a Royal Society Dorothy Hodgkin Research Fellowship. Matt Friedman is thanked for undertaking the X-ray computed microtomography analysis. This study includes data produced in the CTEES facility at University of Michigan, supported by the Department of Earth & Environmental Sciences and College of Literature, Science, and the Arts. TNT was made available with the support of the Willi Hennig Society.

Author Contributions: MDB conceived and designed the study. MDB, AJ, YAA, and EZ participated in all field seasons. RPD and AJ undertook preliminary CT scanning and segmentation that revealed the fossil was a 'placoderm' and had endochondral bone. RS discovered the first vertebrate remains in the first field season at Yamaat Gol in 2010. SG undertook the segmentation of *Minjinia* with input from MDB. AJ performed segmentation of *Diplacanthus* tissue. MC provided input on occipital comparative morphology of 'placoderms'. RPD provided data and comparative analyses and data for endoskeletal tissue. YAA provided background on the geology, palaeontology, and stratigraphy of the type location; EZ and YAA organized field logistics and permitting. MDB, SG, MC, RPD, and AJ undertook the anatomical interpretation and prepared the figures. MDB and SG conducted the phylogenetic analyses. RS conducted the parsimony branch support analyses. TG wrote the script for generating MrBayes partitions from TNT's character fits table and conducted the likelihood and model-fitting analyses. The manuscript was written by MDB, RPD, and SG.

Competing interests statement:

The authors declare no competing interests.

548 **Fig. 1 | MPC-FH100/9.1 a 'placoderm' skull roof and braincase from the Early**
549 **Devonian of Mongolia. a**, Ventral view. **b**, Dorsal view. **c**, Left lateral view. **d**, Posterior
550 view. **e**, Braincase endocavity in dorsal view. Taupe: endoskeleton; grey: mould; blue:
551 exoskeleton. crsp.ri, craniospinal ridge; e.hy.a, sulcus for the efferent hyoid artery; f.m.ep,
552 epaxial muscle fossa; fo.mag., foramen magnum; hy.fo, hyodean fossa; l.d.ao, sulcus for the
553 lateral dorsal aorta; N.V, trigeminal nerve canal; N.VII, facial nerve canal; N.VIII, acoustic
554 nerve canal; nch, notochordal canal; occ.ri, occipital ridge; orb, orbit; pr.pv, paravagal
555 process. Scale bar, 10 mm.
556
557 **Fig. 2 | Endoskeletal mineralisation in fossil gnathostomes. a**, Transverse tomographic
558 slice through MPC-FH100/9.1. **b**, Three-dimensional rendering of trabecular bone structure.
559 **c**, Transverse tomographic section through the braincase of the osteichthyan *Ligulalepis*. **d**,
560 Three-dimensional rendering of the trabecular bone in *Ligulalepis* (**c** and **d** use data from[56]).
561 **e**, Synchrotron tomography image of the calcified cartilage of the certatohyal of the stem-
562 group chondrichthyan *Diplacanthus crassisimus* specimen NMS 1891.92.334. **f**, Semi-
563 transparent three-dimensional structure of calcified cartilage of NMS 1891.92.334. Scale
564 bars, **a** and **b,** 10 mm; **c** and **d**, 1 mm; **e** and **f**, 150 µm.
565
566 **Fig. 3 | Braincase endocavity of *Minjinia*. a,** Semi-transparent rendering of skull roof and
567 braincase (grey and blue) showing extent of endocavity (pink). **b,** Ventral view. **c,** Dorsal
568 view. a.scc, anterior semicircular canal; cav.end, endolymphatic cavity; d.end, endolymphatic
569 duct; h.scc, horizontal semicicular canal; N.V, trigeminal nerve canal; N.VIIhm,
570 hyomandibular branch of facial nerve canal; N.VIIpal, palatine branch of facial nerve canal;
571 N.VIII, acoustic nerve canal; N.X, vagus nerve canal, $N.X_a$, anterior branch of vagus nerve
572 canal; $N.X_p$, posterior branch of vagus nerve canal; occ.a, occipital artery canals; p.scc,

posterior semicircular canal; sac, sacculus; soc, spino-occipital nerve canals; sup.opth, canal for supra-ophtalmic nerve. Scale bars, 10 mm (upper scale bar associates with **a**, lower scale bar associates with **b** and **c**).

Fig. 4 | Strinct consensus tree from parsimony analysis of early gnathostomes showing distribution of endochondral bone and exoskeletal armour. Squares at nodes indicate parsimony reconstruction for endochondral bone. Pie charts at nodes show likelihood reconstructions for the same character under the all-rates-different model (see Extended Data Figs 6 & 7 for competing reconstructions). Grey box indicates uncertainty. Loss of endochondral bone maps closely with generalised loss of bone in chondrichthyans where exoskeletal armour and perichondral bone are also absent.

Table 1 | Tree distribution (n=100) ancestral states estimation results. ER = Equal rates model; ARD = All Rates Different model. The columns AIC and log.like represent the median AIC and log.lik across the 100 parsimony and Bayesian trees (for both models). The like.ratio column is the likelihood ratio for the models compared on these trees. The columns Absent and Present represent the median scaled likelihood for the endochondral bone state.

trees	model	log.like.	like.ratio	AIC	node	Absent	Present
Parsimony	ER	-28.91	4.74	59.82	Minjinia:Gnathostomes	0.67	0.33
(equal weights)	ARD	-26.54		57.09		0.19	0.81
	ER				Crown Gnathostomes	0.91	0.09
	ARD					0.46	0.54
Bayesian	ER	-29.66	5.26	61.32	Minjinia:Gnathostomes	0.73	0.27
(unpartitioned)	ARD	-27.03		58.06		0.17	0.83
	ER				Crown Gnathostomes	0.79	0.21
	ARD					0.22	0.78

591 **Extended Data Fig. 1 | Tomograms of endoskeletal ossification in *Minjinia*.** Top row:
592 semi-coronal sections through braincase. Double-headed arrows indicate anterior-posterior
593 (a-p) dorsal-ventral (d-v) axes. Bottom row: semi-transverse sections through posterior part
594 of endocranium. Voids of black space represent mouldic preservation. Scale bars, 10 mm and
595 apply across each row of panels.
596
597 **Extended Data Fig. 2 | Right orbital wall and innervation pattern of *Minjinia*. a**, orbit in
598 anterolateral view showing disposition of nerve openings (pink infill). **b**, endocast in the
599 same perspective showing the relationship between nerve canals and endocast. a.scc., anterior
600 semicircular canal; $N.V_{2,3}$ trunk of the trigeminal nerve canal for branches 2 and 3; N.VIIhm,
601 hyomandibular branch of facial nerve canal; N.VIIpal, palatine branch of facial nerve canal;
602 sac., sacculus; sup.opth, canal for supra-ophtalmic nerve. Scale bars, 20 mm (upper scale bar
603 associates with **a**, lower scale bar associates with **b** and **c**).
604
605 **Extended Data Fig. 3 | Results of phylogenetic parsimony analysis.** Dataset consists of 95
606 taxa and 284 characters. Both trees are strict consensus topologies. Equal weights parsimony
607 analysis using the ratchet resulted in 240 trees with a length of 831 steps. Implied weights
608 parsimony analysis using random addition sequence + branch-swapping resulted in 8 optimal
609 trees with score 85.20513. Double-digit figures above internal branches are bootstrap values
610 of 50% and over; single-digit figures below branches are Bremer decay index values. Blue
611 shading: osteichthyan total group (dark blue: crown group); orange shading: chondrichthyan
612 total group (dark orange: crown group).
613
614 **Extended Data Fig. 4 | Results of Bayesian phylogenetic analysis using both partitioned**
615 **and unpartitioned data.** Majority-rules consensus trees with posterior probabilities shown

616 along branches. Blue shading: osteichthyan total group (dark blue: crown group); orange
617 shading: chondrichthyan total group (dark orange: crown group).
618
619 **Extended Data Fig. 5 | Likelihood ancestral state mapping of endochondral bone on**
620 **equal weights parsimony results. a**, ARD, all rates different model; **b**, ER, equal rates
621 model.
622
623 **Extended Data Fig. 6 | Likelihood ancestral state mapping of endochondral bone on**
624 **unpartitioned Bayesian analysis results. a**, ARD, all rates different model; **b**, ER, equal
625 rates model.

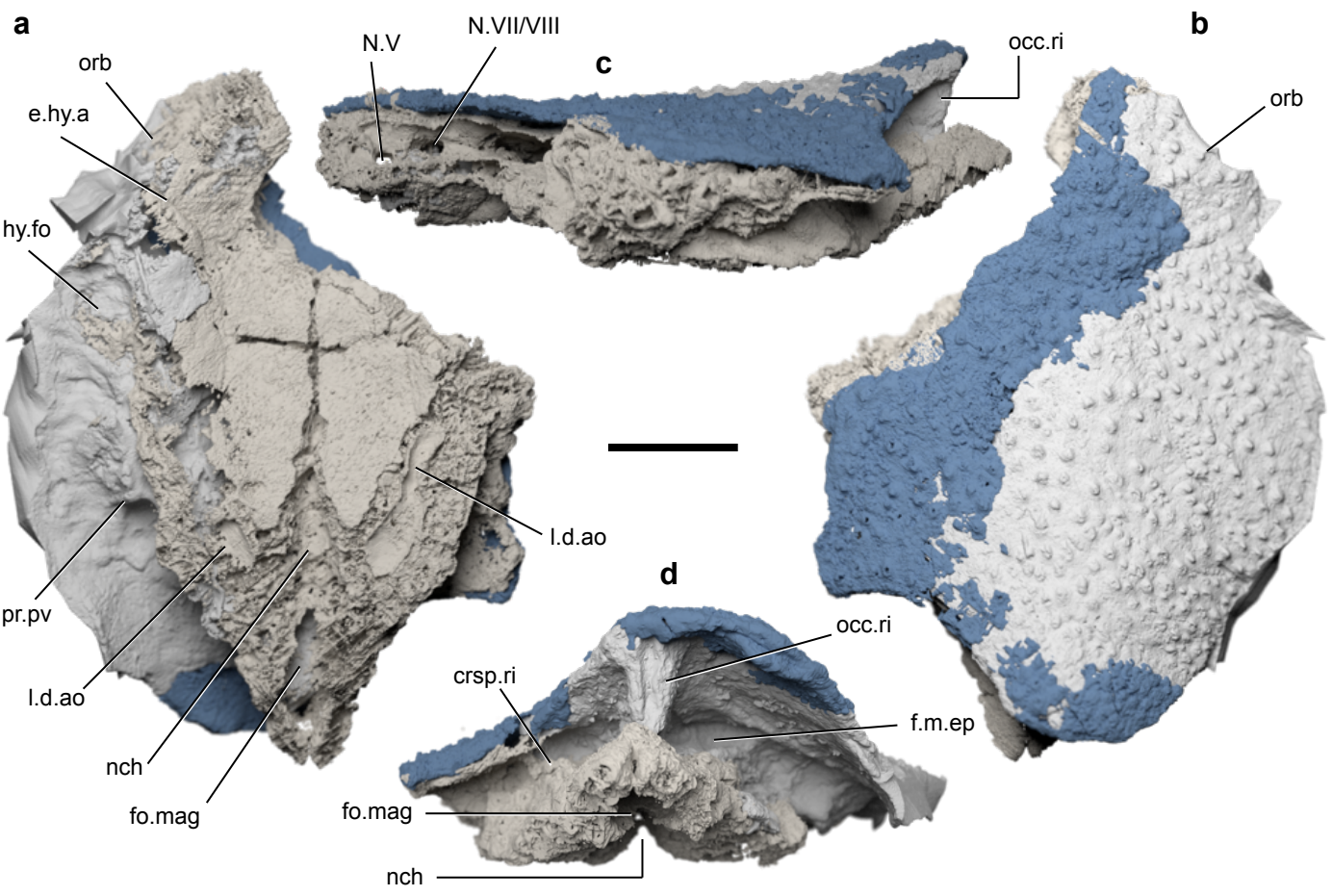
a
orb
e.hy.a
hy.fo
pr.pv
l.d.ao
nch
fo.mag
l.d.ao
c
N.V
N.VII/VIII
occ.ri
b
orb
d
occ.ri
crsp.ri
f.m.ep
fo.mag
nch

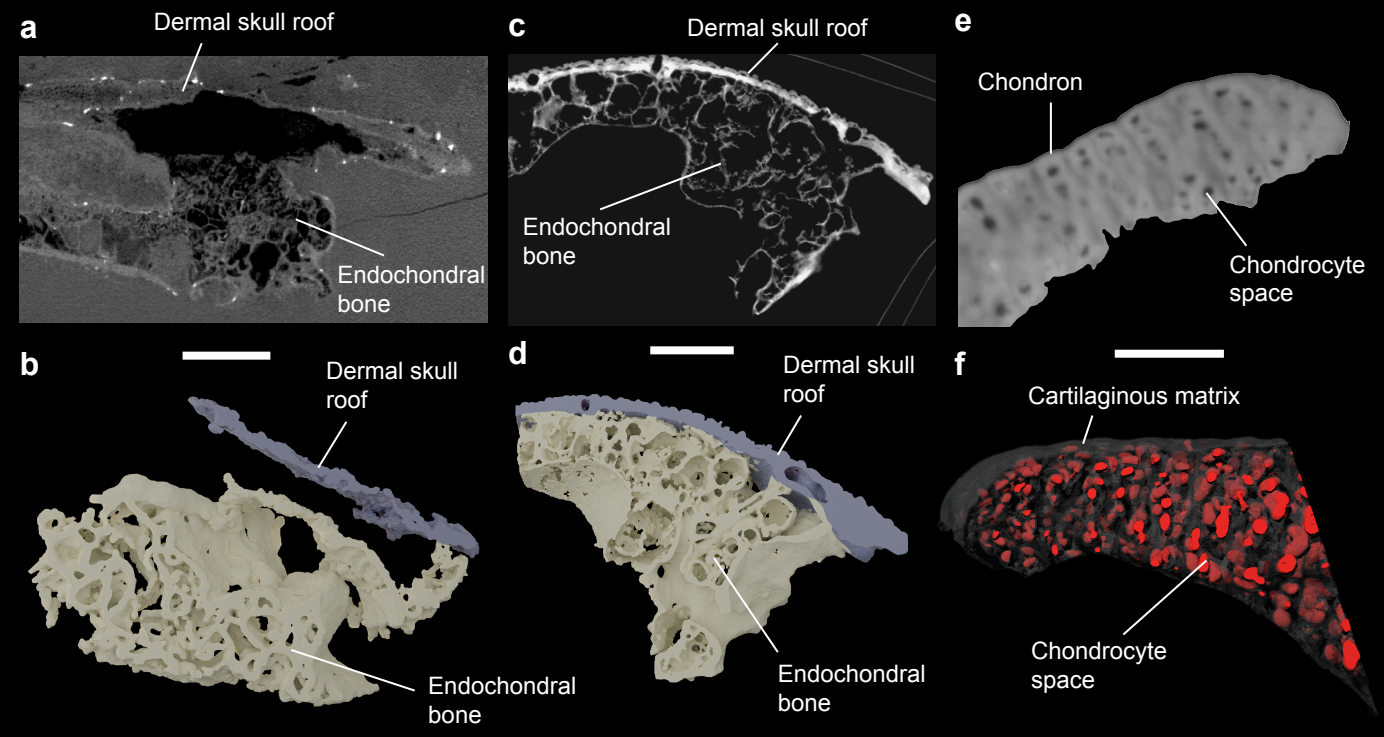
a
Dermal skull roof
Endochondral bone
c
Dermal skull roof
Endochondral bone
e
Chondron
Chondrocyte space
b
Dermal skull roof
Endochondral bone
d
Dermal skull roof
Endochondral bone
f
Cartilaginous matrix
Chondrocyte space

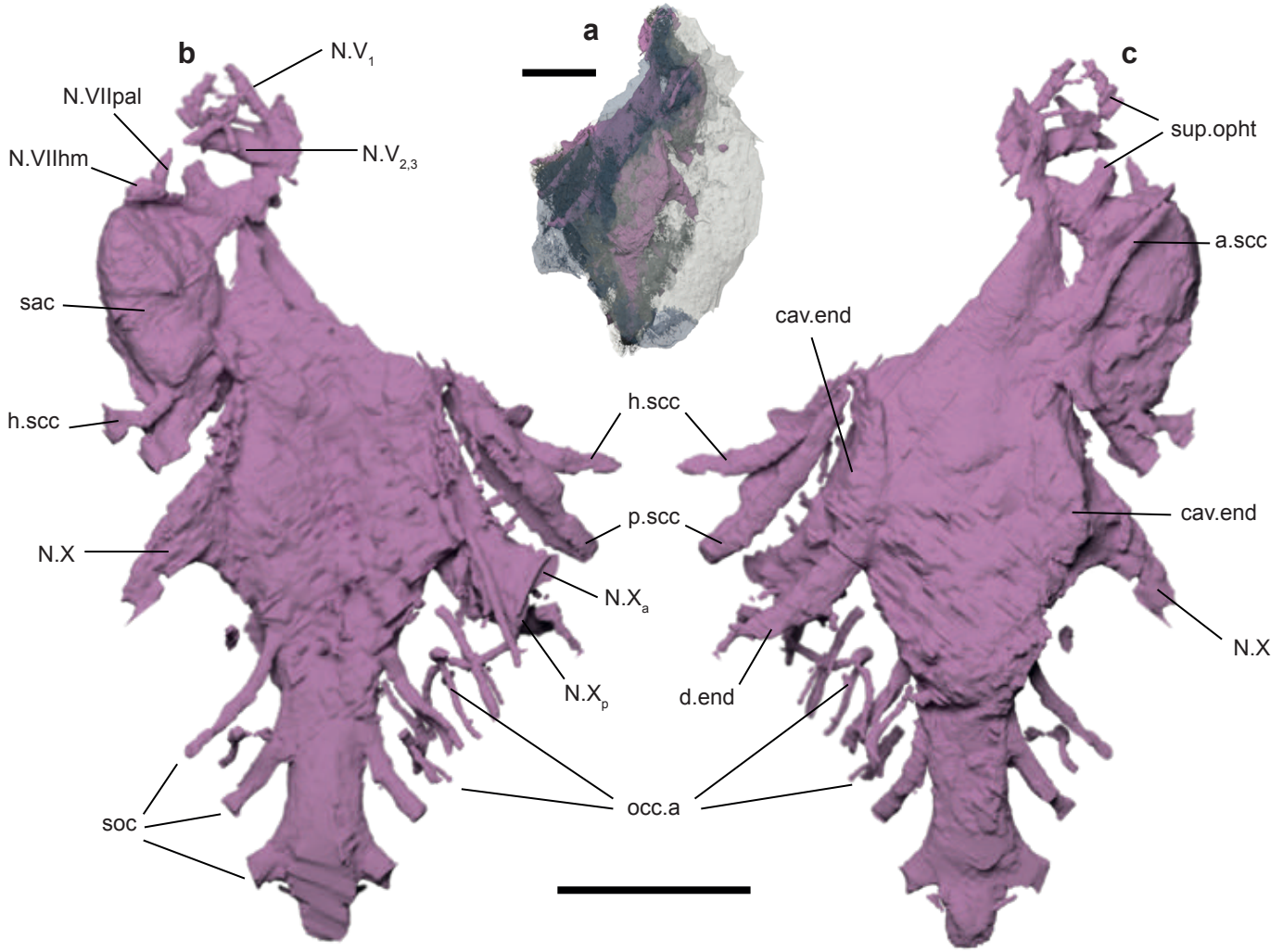
a
b
c
N.V1
N.VIIpal
N.VIIhm
N.V2,3
sac
h.scc
N.X
soc
N.Xa
N.Xp
h.scc
p.scc
occ.a
d.end
cav.end
sup.opht
a.scc
cav.end
N.X

Endochondral bone
Exoskeleton
Absent
Missing / polymorphism
Present
Tessellated
Armoured
Galeaspida
Osteostraci
Gemuendina
Jagorina
Parayunnanolepis
Yunnanolepis
Bothriolepis
Pterichthyodes
Brindabellaspis
Lunaspis
Macropetalichthys
Austroptyctodus
Campbellodus
Rhamphodopsis
Eurycaraspis
Romundina
Kujdanowiaspis
Cowralepis
Dicksonosteus
Buchanosteus
Coccosteus
Incisoscutum
Minjinia
Entelognathus
Ramirosuarezia
Janusiscus
Dialipina
"Ligulalepis"
Guiyu
Sparalepis
Psarolepis
Achoania
Meemannia
Cheirolepis
Howqualepis
Mimipiscis
Raynerius
Moythomasia
Kentuckia
Lawrenciella
Kansasiella
Ptyctolepis
Onychodus
Qingmenodus
Diplocercides
Miguashaia
Gavinia
Styloichthys
Eusthenopteron
Gogonasus
Powichthys
Glyptolepis
Porolepis
Youngolepis
Diabolepis
Dipterus
Uranolophus
Culmacanthus
Tetanopsyrus
Diplacanthus
Gladiobranchus
Ischnacanthus
Poracanthodes
Cassidiceps
Euthacanthus
Mesacanthus
Promesacanthus
Cheiracanthus
Acanthodes
Homalacanthus
Latviacanthus
Brochoadmones
Kathemacanthus
Brachyacanthus
Climatius
Parexus
Ptomacanthus
Vernicomacanthus
Lupopsyrus
Gyracanthides
Obtusacanthus
Pucapampella
Doliodus
Cladodoides
Orthacanthus
Tamiobatis
Akmonistion
Cladoselache
Cobelodus
Tristychius
Hamiltonichthys
Onychoselache
Helodus
Chondrenchelys
Debeerius
Antiarchi
Arthrodira
"Placoderm"
Osteichthyes
Chondrichthyes
Crown-group Gnathostomata

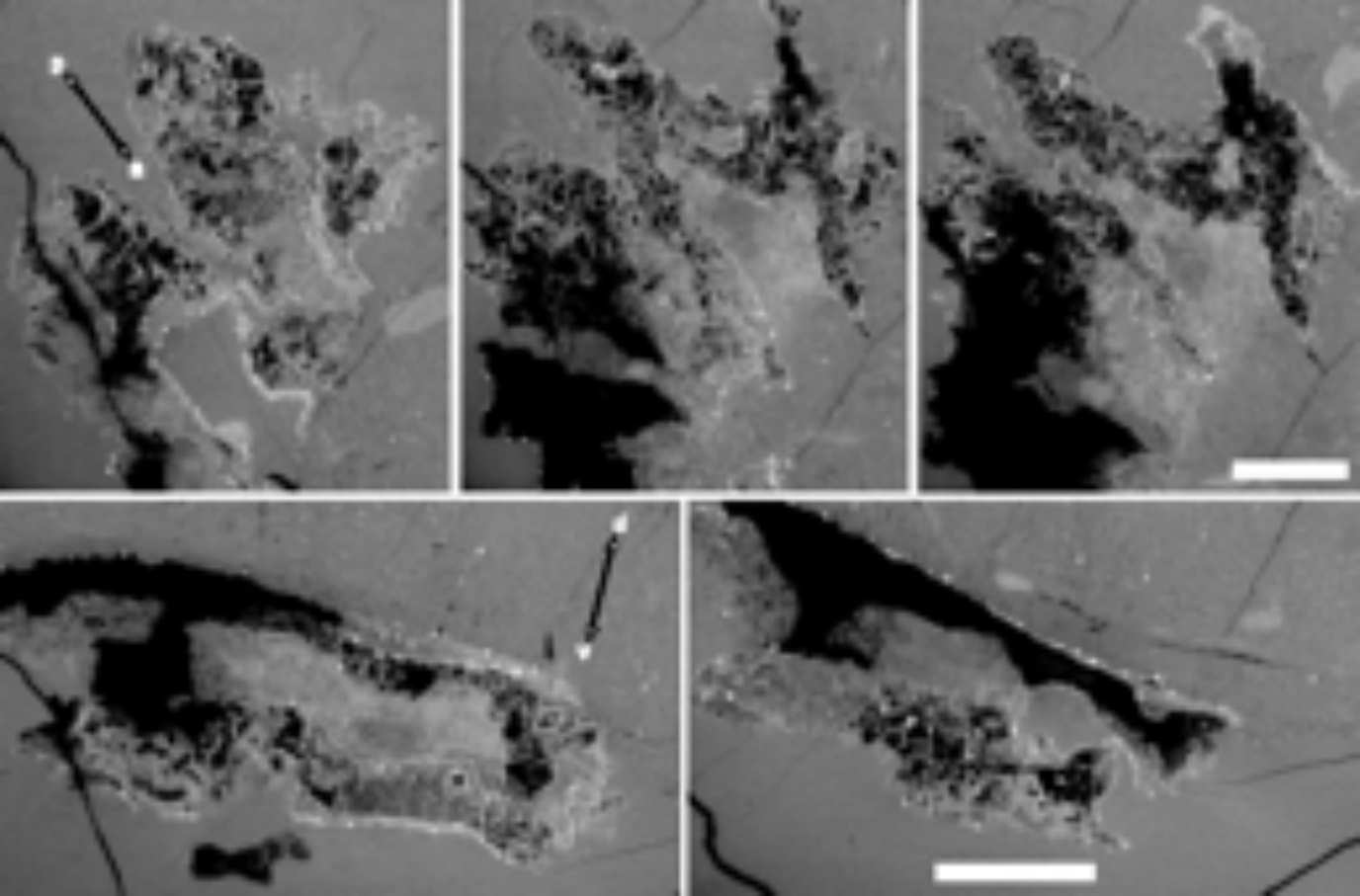

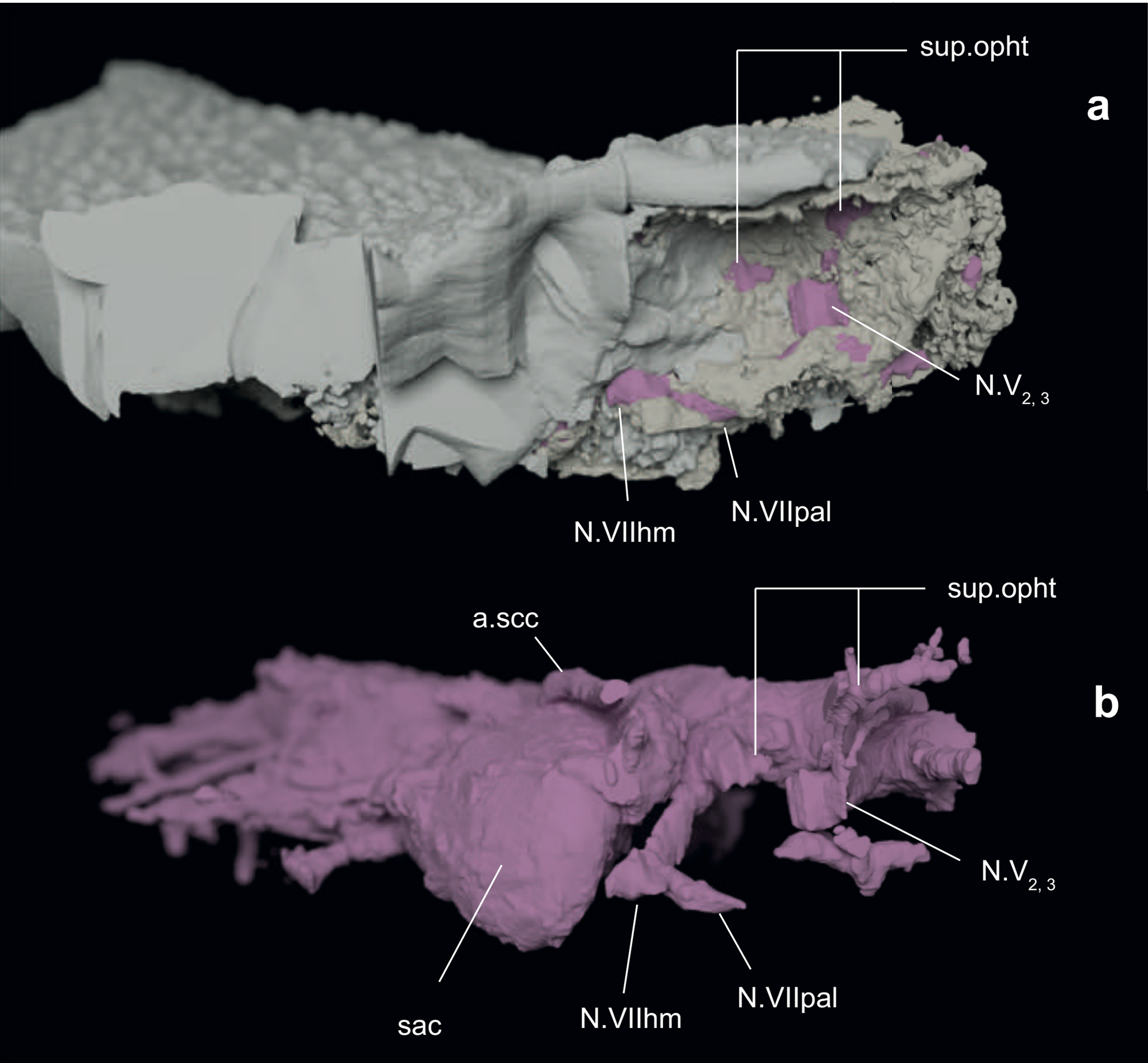
sup.opht
a
N.V2, 3
N.VIIpal
N.VIIhm
sup.opht
a.scc
b
N.V2, 3
N.VIIpal
N.VIIhm
sac

Parsimony: equal weights

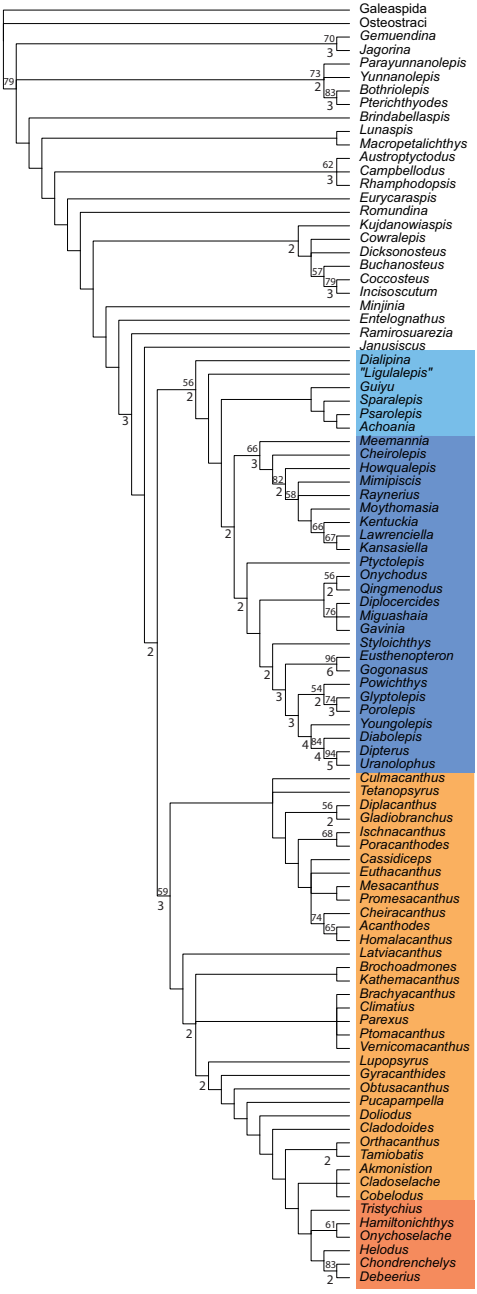

Parsimony: implied weights

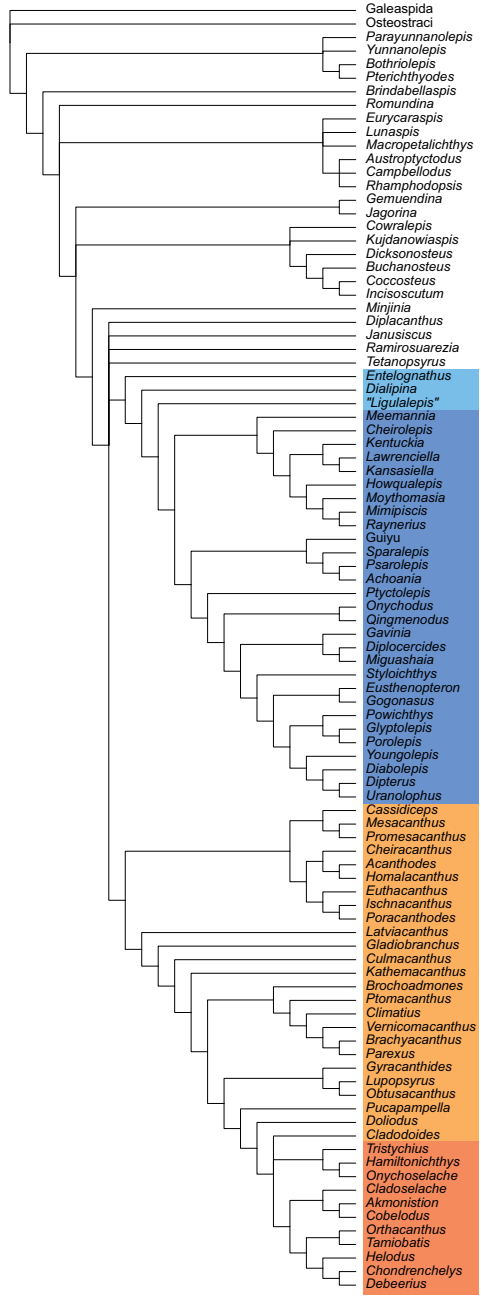

Bayesian: unpartitioned

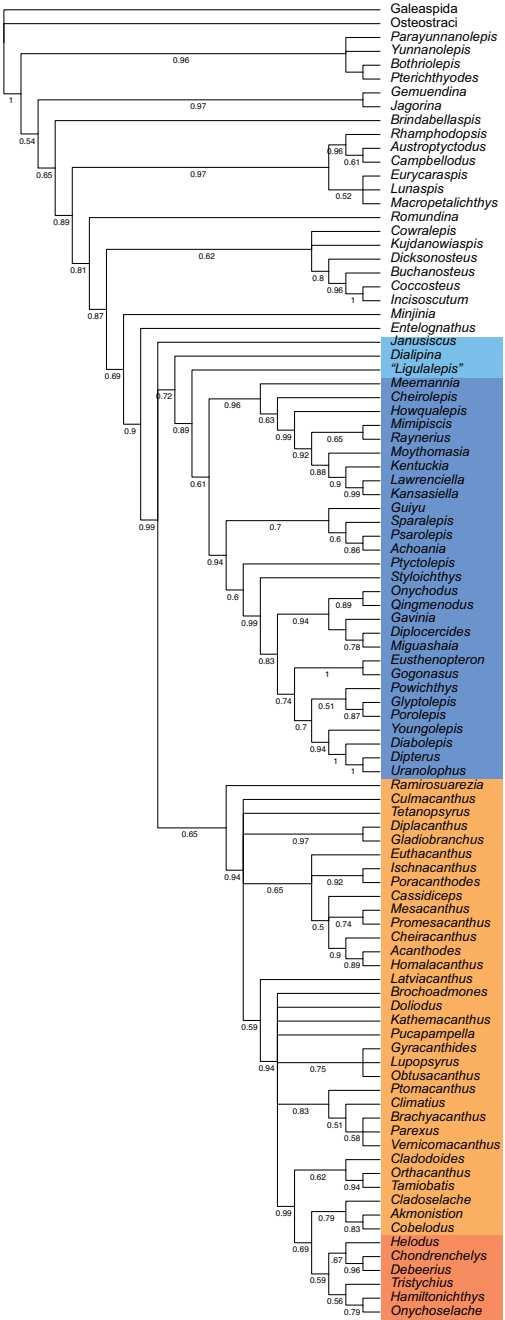

Bayesian: partitioned by character fits

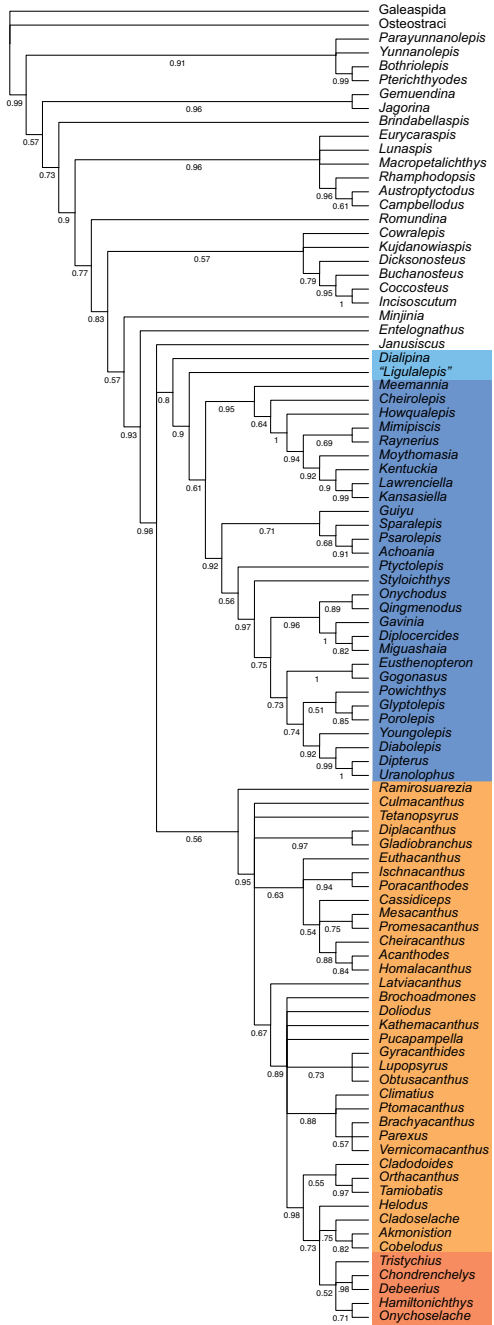

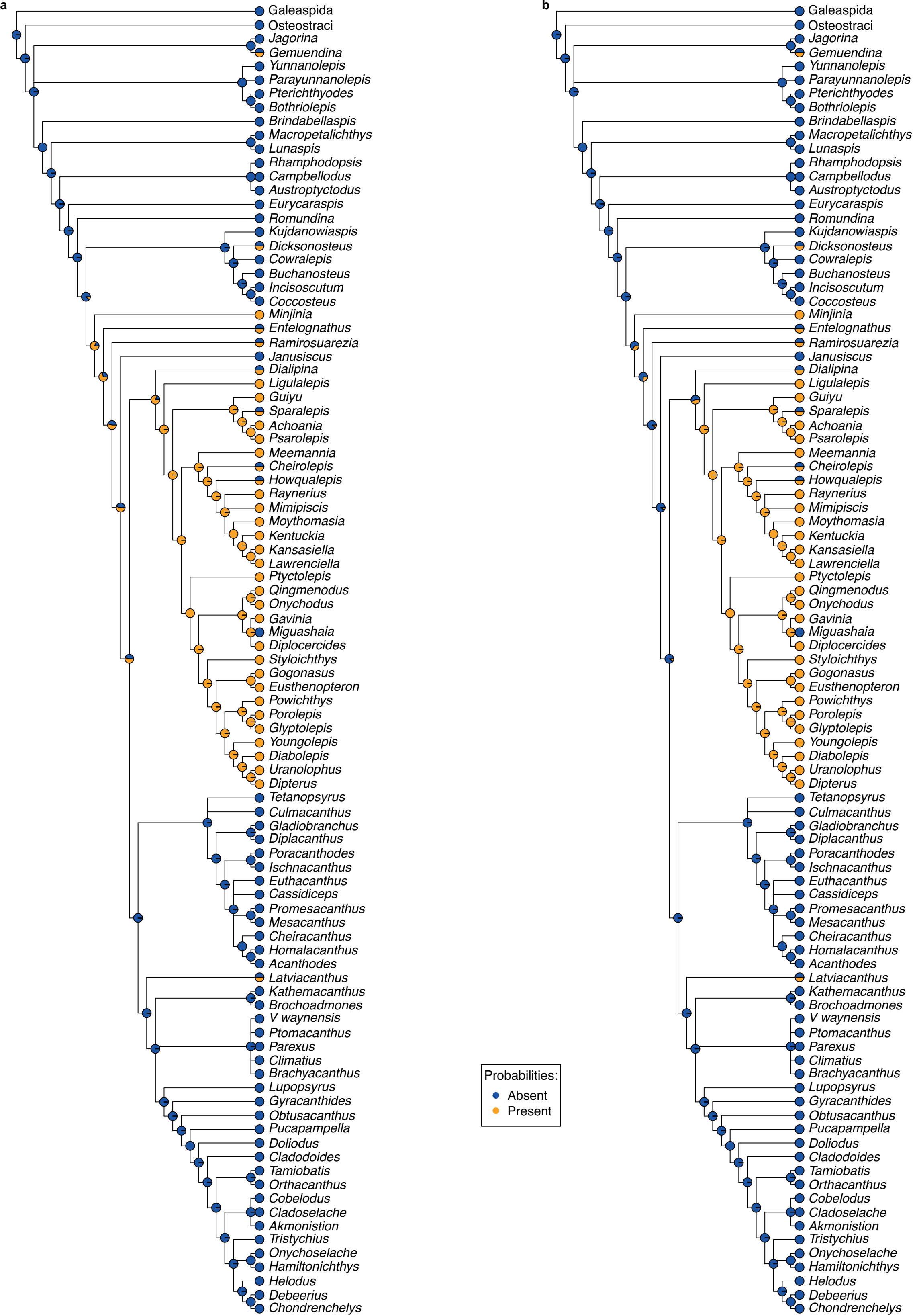
a
b
Galeaspida
Osteostraci
Jagorina
Gemuendina
Yunnanolepis
Parayunnanolepis
Pterichthyodes
Bothriolepis
Brindabellaspis
Macropetalichthys
Lunaspis
Rhamphodopsis
Campbellodus
Austroptyctodus
Eurycaraspis
Romundina
Kujdanowiaspis
Dicksonosteus
Cowralepis
Buchanosteus
Incisoscutum
Coccosteus
Minjinia
Entelognathus
Ramirosuarezia
Janusiscus
Dialipina
Ligulalepis
Guiyu
Sparalepis
Achoania
Psarolepis
Meemannia
Cheirolepis
Howqualepis
Raynerius
Mimipiscis
Moythomasia
Kentuckia
Kansasiella
Lawrenciella
Ptyctolepis
Qingmenodus
Onychodus
Gavinia
Miguashaia
Diplocercides
Styloichthys
Gogonasus
Eusthenopteron
Powichthys
Porolepis
Glyptolepis
Youngolepis
Diabolepis
Uranolophus
Dipterus
Tetanopsyrus
Culmacanthus
Gladiobranchus
Diplacanthus
Poracanthodes
Ischnacanthus
Euthacanthus
Cassidiceps
Promesacanthus
Mesacanthus
Cheiracanthus
Homalacanthus
Acanthodes
Latviacanthus
Kathemacanthus
Brochoadmones
V waynensis
Ptomacanthus
Parexus
Climatius
Brachyacanthus
Lupopsyrus
Gyracanthides
Obtusacanthus
Pucapampella
Doliodus
Cladodoides
Tamiobatis
Orthacanthus
Cobelodus
Cladoselache
Akmonistion
Tristychius
Onychoselache
Hamiltonichthys
Helodus
Debeerius
Chondrenchelys
Probabilities:
Absent
Present

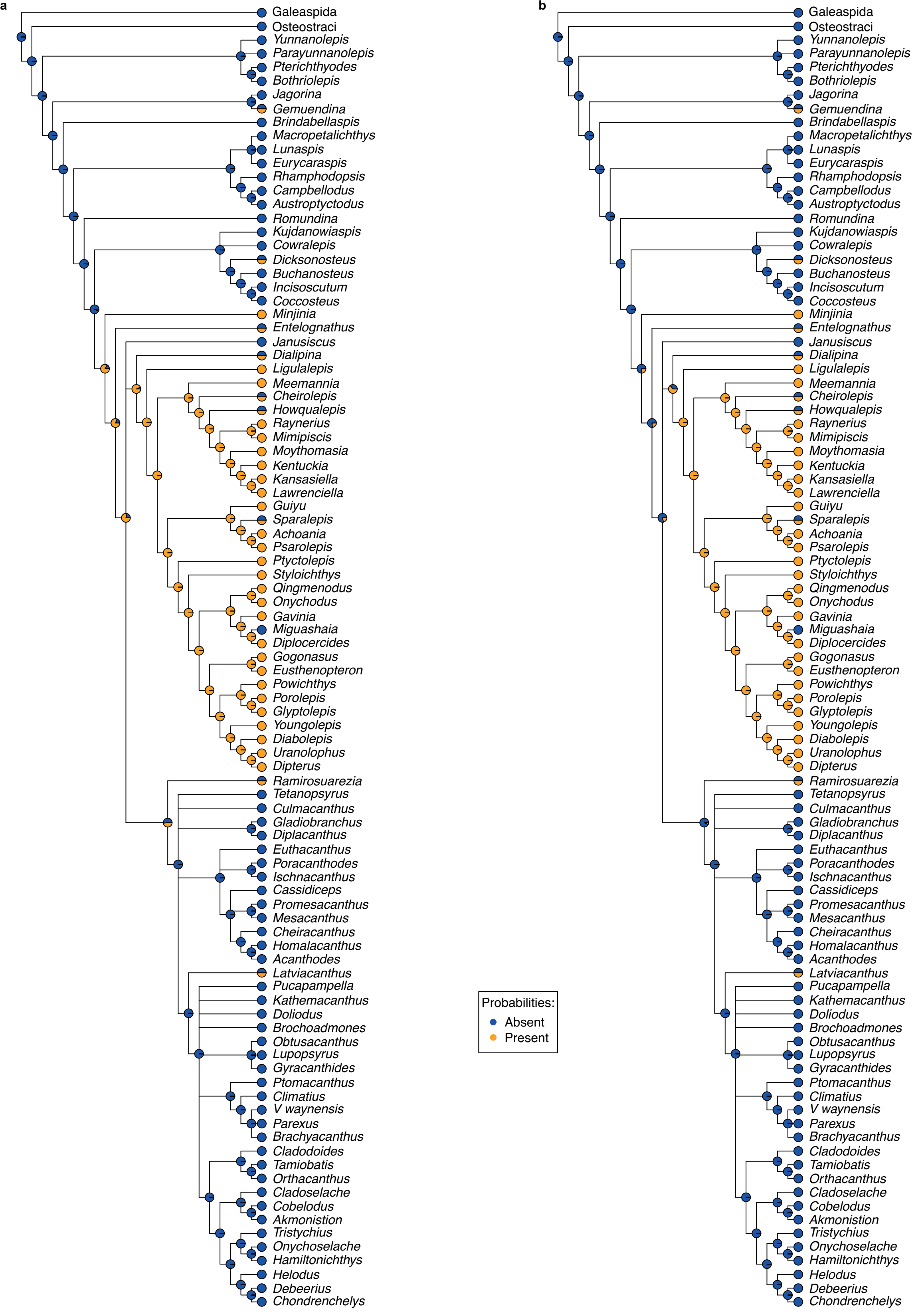
a
b
Galeaspida
Osteostraci
Yunnanolepis
Parayunnanolepis
Pterichthyodes
Bothriolepis
Jagorina
Gemuendina
Brindabellaspis
Macropetalichthys
Lunaspis
Eurycaraspis
Rhamphodopsis
Campbellodus
Austroptyctodus
Romundina
Kujdanowiaspis
Cowralepis
Dicksonosteus
Buchanosteus
Incisoscutum
Coccosteus
Minjinia
Entelognathus
Janusiscus
Dialipina
Ligulalepis
Meemannia
Cheirolepis
Howqualepis
Raynerius
Mimipiscis
Moythomasia
Kentuckia
Kansasiella
Lawrenciella
Guiyu
Sparalepis
Achoania
Psarolepis
Ptyctolepis
Styloichthys
Qingmenodus
Onychodus
Gavinia
Miguashaia
Diplocercides
Gogonasus
Eusthenopteron
Powichthys
Porolepis
Glyptolepis
Youngolepis
Diabolepis
Uranolophus
Dipterus
Ramirosuarezia
Tetanopsyrus
Culmacanthus
Gladiobranchus
Diplacanthus
Euthacanthus
Poracanthodes
Ischnacanthus
Cassidiceps
Promesacanthus
Mesacanthus
Cheiracanthus
Homalacanthus
Acanthodes
Latviacanthus
Pucapampella
Kathemacanthus
Doliodus
Brochoadmones
Obtusacanthus
Lupopsyrus
Gyracanthides
Ptomacanthus
Climatius
V waynensis
Parexus
Brachyacanthus
Cladodoides
Tamiobatis
Orthacanthus
Cladoselache
Cobelodus
Akmonistion
Tristychius
Onychoselache
Hamiltonichthys
Helodus
Debeerius
Chondrenchelys
Probabilities:
Absent
Present